Solvent-induced single-chain conformations of a linear synthetic polymer

Susil Baral[1,*], Binod Gautam[1]

[1]Department of Chemistry, Illinois State University, Normal IL 61790, USA

* Correspondence: sbaral1@ilstu.edu

Supplementary information

S1. Materials and chemicals

The chemicals including norbornene (N32407), second-generation Grubbs catalyst (569747), and anhydrous toluene (244511) were purchased from Sigma Aldrich and used as received. The norbornene-silane reagent ([(5-bicyclo [2.2.1] hept-2-enyl) ethyl] trimethoxysilane) was purchased from Gelest (SIB0988.0). Carboxylic acid functionalized magnetic particles of 1 μm diameter (Dynabeads MyOne Carboxylic Acid, Invitrogen, 65001) were purchased from Thermo Fisher Scientific. All manipulations of air and moisture-sensitive compounds were carried out under argon or nitrogen protection using standard Schlenk line techniques.

S2. Synthesis of surface-grafted polymers

Our experimental approach of synthesizing surface-grafted polymers for single-molecule manipulations involves three steps as illustrated in **Fig. S1**.

I. Beads preparation: The carboxylate functional groups on the magnetic particles (Dynabeads MyOne Carboxylic Acid, Invitrogen, 65001, 1 μm) were first converted into silver-carboxylates by performing a deprotonation reaction of 100 μL stock solution of magnetic particles with 0.5 mL 10^{-2} M NaOH under stirring for about 2 hours. The particles were precipitated under centrifuge and washed 5 times using DI water to remove unreacted NaOH. This was followed by the addition of 1 mL 10^{-3} M $AgNO_3$ solution to the particles. The mixture was stirred for about 2 hours, and the particles were washed an additional 5 times using DI water to remove unreacted $AgNO_3$. The particles were dried under vacuum for several hours and a dilute solution (1mg/mL) of second-generation Grubbs catalyst (G2) was added for the catalyst functionalization to magnetic particles via substitution of a chloride ligand in an airtight vial (Chemglass, CG-4908-01) under argon. After 3-4 hours of reaction under constant stirring, the magnetic particles were precipitated using a magnet, and the particles were washed 6-8times with dry toluene to remove any unfunctionalized or non-specifically attached G2 catalyst.

(II) Surface preparation: Glass coverslips (VWR, 48393-106) were first cleaned by sonication in a detergent solution. Position markers were immobilized for drift correction by drop-casting a dilute solution of the regular (unfunctionalized) magnetic particles onto the clean surface. The coverslip surface was further functionalized with norbornene molecules using commercially available Norbornene silane reagent ([(5-bicyclo[2.2.1]hept-2-enyl)ethyl]trimethoxysilane; Gelest, SIB0988.0) *via* vapor reaction overnight. A flow cell with inert gas protection was subsequently constructed using the functionalized coverslips as reported previously[1-3].

(III) Bead immobilization and polymer growth: The G2 functionalized magnetic particles were dispersed in dry toluene and introduced in the flow chamber made using norbornene functionalized glass slides, resulting in tethering of the particles to the surface via metathesis reaction between surface norbornene and G2 immobilized onto the magnetic particle. A monomer solution (250 μL

1 M norbornene in dry toluene) was then introduced to allow the growth of surface-grafted polymers for about an hour. The polymerization reaction was stopped by flushing out the norbornene monomer and filling the flow chamber with toluene, resulting in the polymers with one end tethered to the glass coverslip surface and the other end attached to the magnetic particles for magnetic tweezers manipulations.

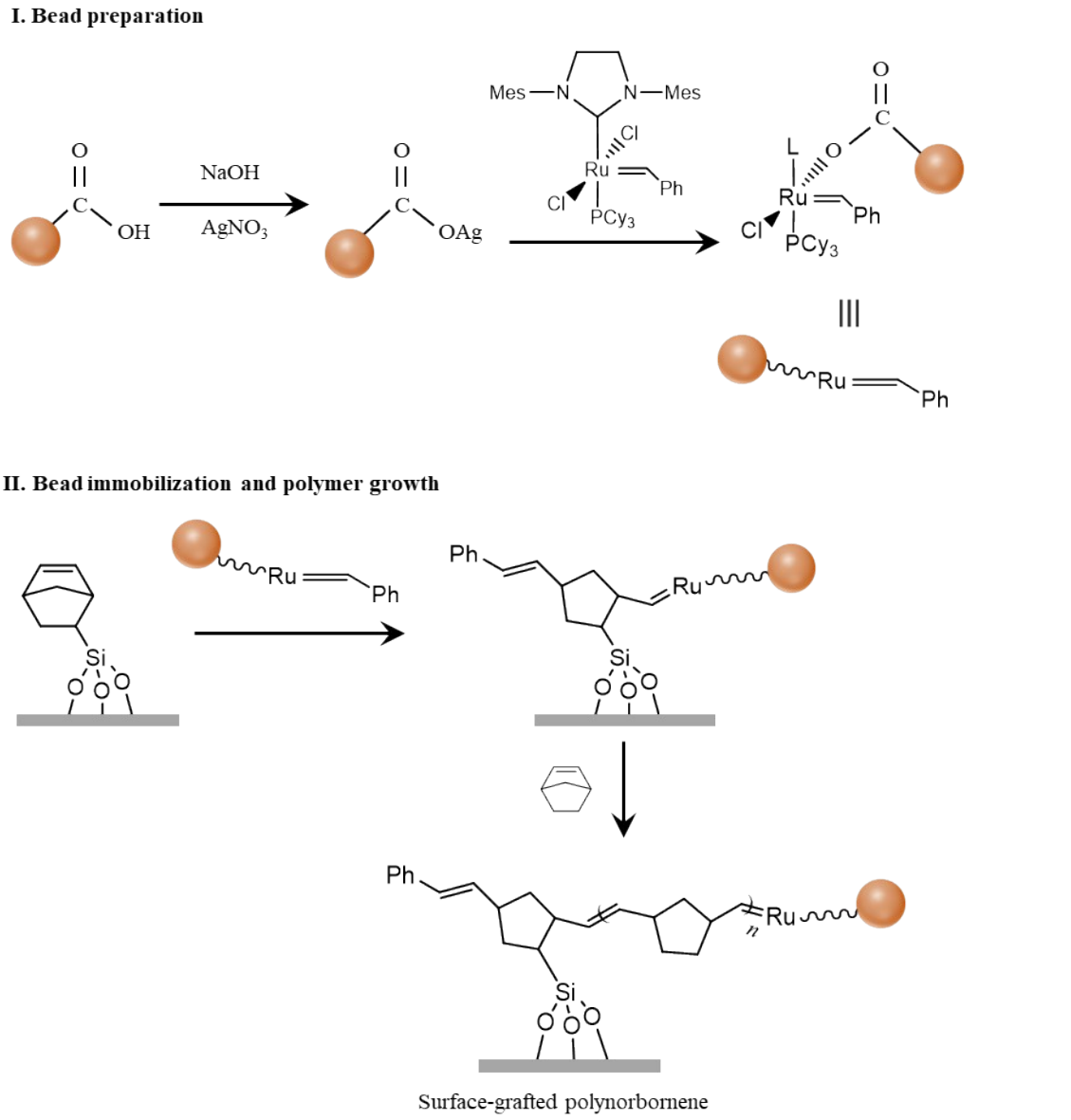

Fig. S1. Experimental scheme of growing surface-grafted polynorbornene for single-molecule manipulations. NOTE: L in the simplified scheme in step I represents NHC ligand and the catalyst immobilized bead from step I is presented in a simplified form in surface immobilization step II.

S3. Proof-of-principle measurements to validate polymer growth via catalyst immobilized onto the magnetic particles

We performed proof-of-principle measurements to validate our experimental scheme of growing surface-grafted polymers as proposed in **Fig. S1**. **Fig. S2** shows the SEM/EDS images of the magnetic particles after catalyst functionalization. The pictures on the bottom show the elemental mapping of Fe (green, left) and Ru (blue, right) for the highlighted region on the top survey image. The elemental map of Fe is consistent with the particle structure as it is made of iron oxide nanoparticles. The Ru mapping is not very distinct due to the low relative abundance of surface-immobilized Grubbs catalyst but appears to be consistent with the particle outline from the Fe map.

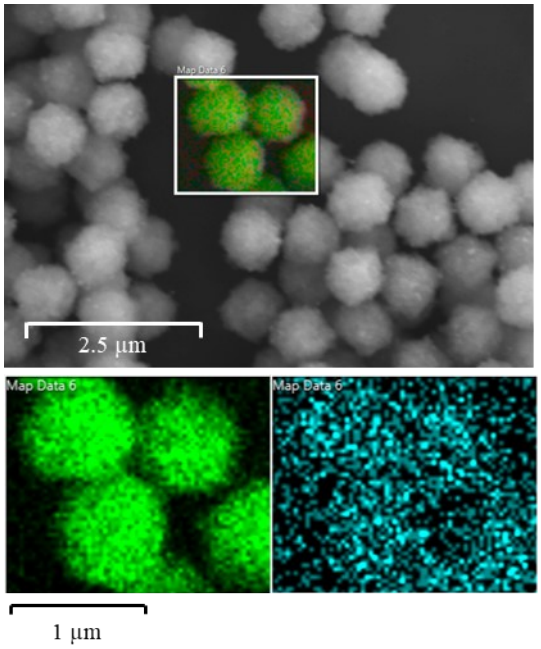

Fig. S2. SEM/EDS images of magnetic particles.

We further used the catalyst-functionalized magnetic particles shown in **Fig. S2** to grow particle-grafted polymers to validate our proposed scheme. The polymerization reaction was performed using 1 M norbornene monomer in toluene solvent under argon protection. During the polymerization, the solution turned viscous in about 60 minutes and formed a gel in about 2 hours. **Fig. S3** shows the image of a reaction vial with a distinct polymer film after drying the solvent. A control vial with magnetic particles without Grubbs catalyst functionalization does not turn viscous nor forms a polymer film after drying. This confirms the polymer film in **Fig. S3** is grown from Grubb's catalyst immobilized onto the magnetic particles and validates our proposed scheme of growing surface-grafted polymers for real-time growth study.

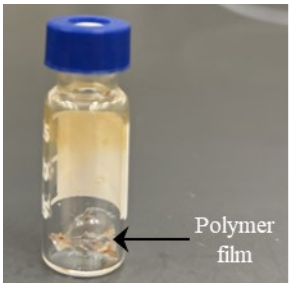

Fig. S3. Polymer film grown from Grubbs catalyst immobilized onto the magnetic particles.

In a separate measurement, we used ethyl vinyl ether to cleave the polymer after 60 minutes of polymerization reaction, separated the magnetic particles using the magnet, and precipitated the supernatant in ethanol in the separate vial. The precipitate was dried in vacuum and ^{1}H NMR measurement was performed in $CDCl_3$. The NMR spectrum as shown in **Fig. S4** resembles exactly with the NMR spectrum of polynorbornene separately polymerized using regular Grubbs catalyst.

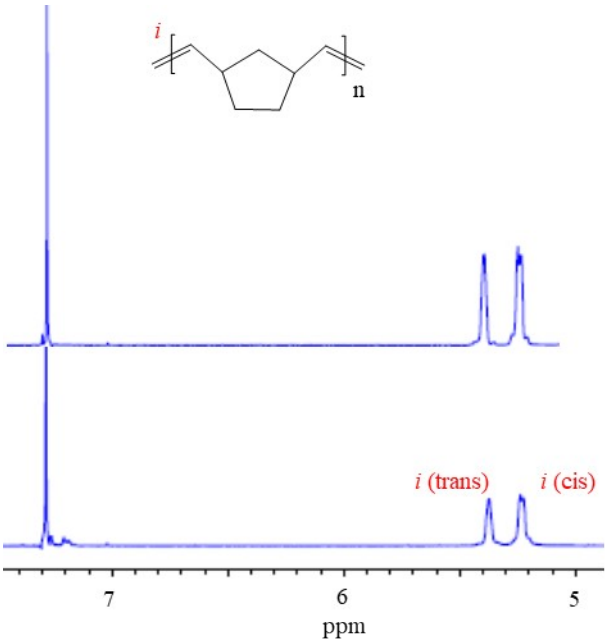

Fig. S4. ^{1}H NMR spectrum in $CDCl_3$ of regular ensemble polymerization using G2 and norbornene to form polynorbornene (bottom) in comparison with that of polynorbornene grown and cleaved off the G2 immobilized magnetic particles (top).

S4. Magnetic tweezers (MT) microscopy

A schematic of our MT setup is shown in **Fig. S5**. The setup is custom built on top of an Olympus IX73 inverted microscope platform and mounted on a laser table (Thorlabs, T48H) with active vibration isolation legs (PTS602).

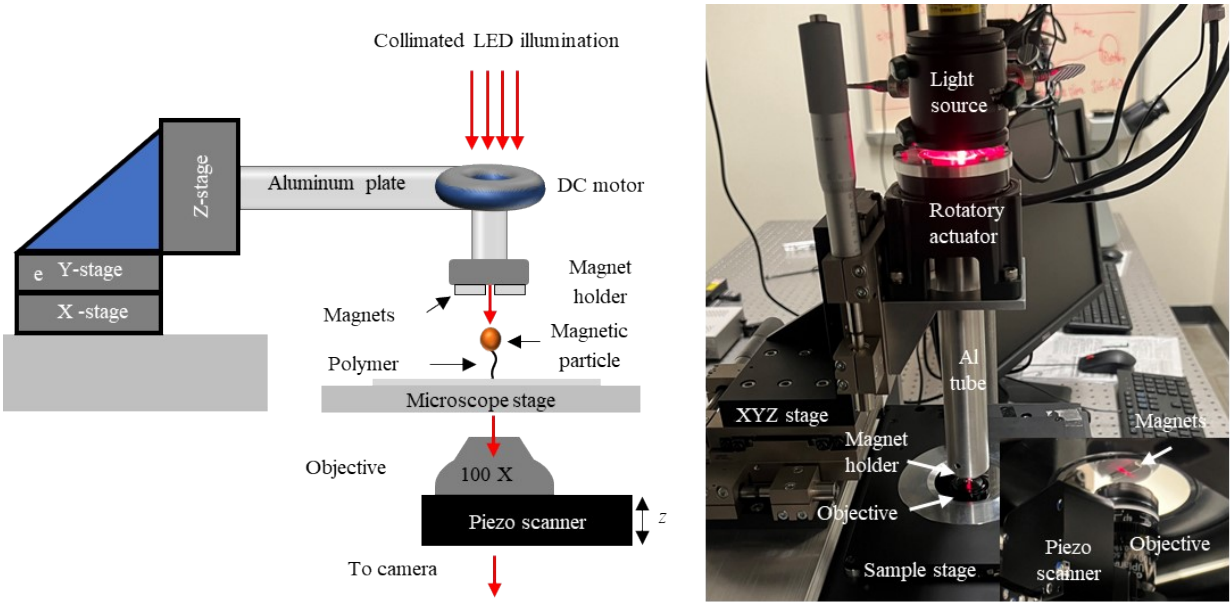

Fig. S5. Schematic (left) and the photograph (right) of our magnetic tweezers setup. The inset on the bottom right is the picture from underneath the microscope showing the objective attached to a piezo scanner below the stage, the magnet holders with the horizontal orientation of magnets, and the light coming through the gap between the magnets.

Two rectangular magnets (Pacific PAC Technologies; N52-5×3×8 mm; NdFeB; Ni-plated) are placed in a horizontal configuration with ~ 0.7 mm gap on a custom-built aluminum magnet holder. The magnet holder is fixed to the bottom end of the aluminum tube using thread screws, and the top end of the aluminum tube is attached to a hollow rotatory actuator (Oriental motor, DGB85R12-AZACL). The actuator is anchored to a translational stage (Thorlabs, LNR 50M) via custom machined aluminum plate. The translational stage controls the movement of the magnets in three dimensions with micrometer precision. The rotational movement of the magnets is controlled by the driver (Oriental Motor, AZD-AD) connected to an actuator. The optical axis of microscope and the rotational axis of the magnets in the lateral plane are manually aligned by adjusting the *x* and *y*-position of magnets using the translational stage. The optimal alignment is achieved when the rotation of magnets does not alter the brightness of the field-of-view.

The sample is mounted on the microscope sample stage (Olympus, IX3-SVL) and the illumination is provided by the collimated LED lights (Thorlabs, M660L4-C1, 660 nm) mounted above the rotatory actuator. The illumination can reach the sample by passing through the hollow end of the actuator, the aluminum tube, and the gap between the magnets. Imaging is performed in bright-field transmission mode using a 100× oil-immersion objective (OLYMPUS PL APO 100X TIRF Objective, NA 1.50), and the images are recorded by a CMOS camera (Infinity 8-2M) at 50-100 frames per second rate. The objective is mounted on a piezo nanofocusing system (Physik Instrumente, P-725.1CDE2) that allows control of the objective/sample position in lateral direction with nm precision for *z*-position calibration.

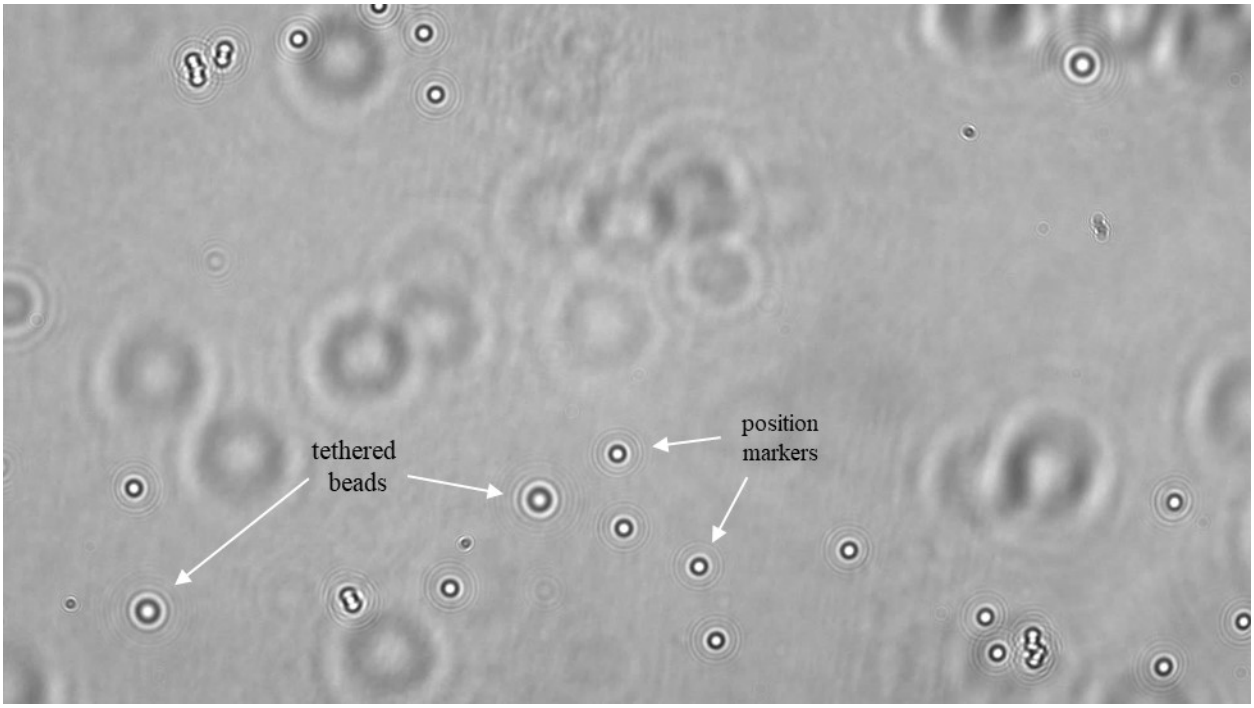

Fig. S6. Brightfield optical transmission image of a typical field of view showing position markers and tethered particles.

The lateral (*xy*) and axial (*z*) position of a magnetic particle during MT measurements is determined by analyzing the bright field transmission images of the magnetic particles using the method described in detail previously[1-3]. The custom-written MATLAB scrips for the 3D position

tracking with nm precision are already published as a supplemental information of a manuscript previously[2].

The refractive indices of the toluene-ethanol mixtures were determined using the Arago-Biot rule, considering the mole fraction and molar volumes of toluene and ethanol. The resulting values listed in **Table S1** were utilized for the *z*-position measurement.

Table S1. Refractive indices of the solvents used in z-position measurements.

Solvent	Refractive index
Toluene	1.500
Tol:EtOH (9:1)	1.486
Tol:EtOH (8:2)	1.472
Tol:EtOH (7:3)	1.458
Tol:EtOH (6:4)	1.444

S5. Force calibration of the MT setup

The vertical force (F) exerted on the polymer tether is calibrated by tracking the motions of the magnetic particle in the xy plane and using the fluctuation-dissipation theorem, $F = k_B TL/\langle \Delta x^2 \rangle$, where k_B is the Boltzmann constant, T is temperature, L is the tether end-to-end extension distance and $\langle \Delta x^2 \rangle$ is the variance of the transversal position of the particle along the magnetic field direction[1, 4-6]. The end-to-end extension distance of a polymer (L) is determined by the z position of the magnetic particle relative to the z position where the particle is on the glass surface. The variance, $\langle \Delta x^2 \rangle$ is determined by tracking the x position of the magnetic particle in the x-vs-time trajectory. For force calibration and force-extension measurements, a torsional force is applied to the field of view by rotating the magnets, which allows for the differentiation of single-polymer or multi-polymer tethers between the particle and the surface. Only the former allows for free rotation [**Fig. S7(a)**], while the latter restrains it.

NOTE: We do not have precise control over the density of the catalyst functionalized to the magnetic particles (step I, Fig. S1). Therefore, some magnetic particles may have many catalysts immobilized onto them, while others may have none. Furthermore, the magnetic particle could be immobilized on the surface through a single or multiple tethers (step II, Fig. S1). While we do not have control (or quantification) over this, we can differentiate whether the magnetic particle is tethered to the surface via single or multiple polymers after growth through magnet rotation (i.e., though there may be more than 1 polymer-chain attached at other regions of the magnetic particle surface, we are only stretching and studying the elasticity of a single-chain). We observe circular precession movements for a magnetic particle tethered to the surface via a single polymer tether [e.g., Fig. S7(a)], which allows us to locate single chains for force-extension measurements. In practice, we observe heterogeneity in the proportion of single-and multi-polymer tethered particles in any given flow cell. We perform a survey scan of the flow chamber, identify the region with single-polymer tethered particles, and perform single-chain elasticity experiments.

Since the configuration of the magnets is fixed, the magnetic force is calibrated at different magnet positions (i.e., different distances between the magnets and the tethered particles) along the z direction [**Fig. S7(b)**]. In changing the magnetic force, the magnet position is changed by moving

the magnet holder in the *z* direction with a 50 μm step size, controlled by the micro-stage. The thickness of the flow cell in our measurements is almost constant and the position at which the magnets nearly touch the upper surface of the flow cell is assigned as the zero-magnet distance (i.e., z-position with the highest accessible force). The magnetic force follows exponential decay. For consistency, the data were fitted with the exponential function and the best-fit values from the exponential profile were used as the Force in subsequent analysis of the force-extension data.

The calibration of magnetic force vs. magnet positions was performed on several single tethers, and one of the representative calibrations was used as the common force for all molecules. We have found the variation in determined magnetic force is within 10% for individual tethers within the field of view, which is within the error of magnetic force determination[1]. This minute variation

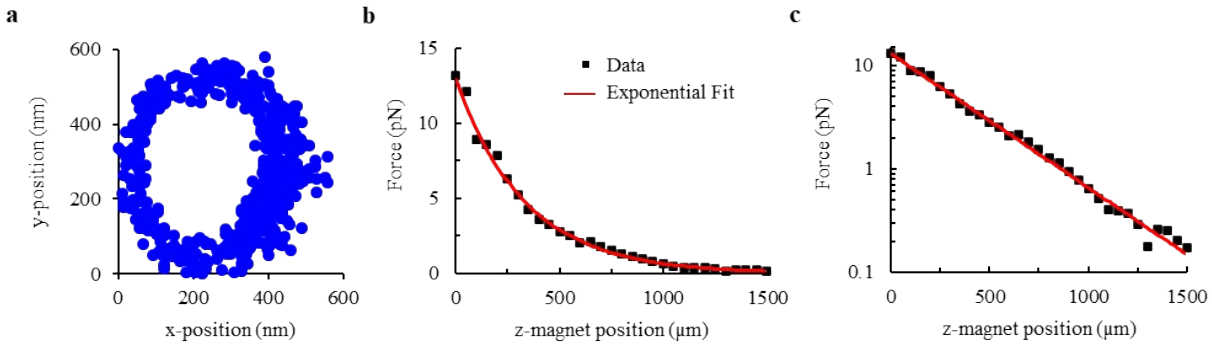

Fig. S7. (a) Representative x-y position map of a single-polymer tethered magnetic particle showing circular precession movements under magnet rotation. (b) Representative magnetic force vs. z magnet distance data. The magnetic force F is determined based on the fluctuation-dissipation theorem (black dots, equation in the text above) and fitted with a single-exponential function (red curve). (c) Magnetic force in log scale vs. z magnet position data (same data as in b), confirming the exponential fit describes the data well down to the low force end (i.e., 0.1 pN).

does not affect the overall single-chain elasticity and scaling behavior[7].

S6. Rationale against bond breakage at the attachment point in our single-chain elasticity measurements

In our experimental scheme (**Fig. S1**), the polymer is attached at both ends (i.e., magnetic particle and the surface) via covalent interactions whose strength is expected to be of the order of nN[1, 8]. The highest force applied in our measurements is only 13 pN, which is more than two orders of magnitude less than the strength of a typical covalent bond, and bond cleavage is much less likely. Additionally, if a bond cleaves at the attachment point, the magnetic particle will become loose and either diffuse out of the field of view or crash onto the flow chamber surface. Any of these instances can be easily identified during the force-extension measurements and mark the end of the data collection. Bond cleavage at the attachment point can occur during living polymerization experiments[1], and tether peeling off the surface may occur in measurements involving higher forces (~100 pN) and a non-specific tether attachment scheme[9]. Since our attachment scheme is covalent, polymerization is completed prior to the force-extension measurements, and the force range in our measurements is very low, we can rule out the possibility of bond cleavage at the attachment point.

S7. Analysis of force-extension data

The analysis of the experimental force-extension data was performed using a self-consistent scheme described in detail previously. The custom-written MATLAB codes for the analysis of the force-extension data were published as supplemental information in a manuscript previously[2].

Briefly, the high force region $\left(f > \frac{k_B T}{2p}\right)$ of the data was fitted with the worm-like chain (WLC) model equation, $f = \frac{k_B T}{p}\left[\frac{1}{4}\left(1 - \frac{L}{L_0}\right)^{-2} - \frac{1}{4} + \frac{L}{L_0}\right]$ to extract the persistence length, p and the contour length, L_0 of the polymer. The low force region $\left(f < \frac{k_B T}{2p}\right)$ of the data was fitted with power law equations of the general form $L/L_0 = mf^{\gamma}$ to extract the scaling exponents (γ). For consistency, our fitting algorithm evaluates if the entire data in the low force range ($f < f_{HF}$) can be represented by a single scaling regime or requires two distinct scaling regimes with a crossover force (f_c) based on the confidence intervals of the one regime or two regime fitting[2].

It is important to note that we only study relatively long polymers in our single-chain measurements, as the uncertainties associated with extension measurements are higher for shorter polymer chains with extension less than the size of the magnetic particle (which is about 1 μm)[2].

In the example shown in **Fig. S8** [singe-chain data for the polynorbornene in 9:1 toluene-ethanol mixture, gray data in **Fig. 2(a)**] self-consistent, iterative worm-like chain (WLC) fitting of the data (black stars and dashed black curve) at $f > f_{HF}$ yields the persistence length (p = 0.86 ± 0.03 nm), contour length (L_0 = 5485 ± 70 nm) and the f_{HF} value (= $k_B T/2p$ = 2.35 pN). The data at $f < f_{HF}$ shows a deviation from the WLC fit and requires two distinct scaling regimes with the crossover force (f_c) at 0.87 pN. The data between 2.35 pN and 0.87 pN display swollen chain behavior with a scaling exponent of 0.73 (which is consistent with the Pincus prediction of $L/L_0 \sim f^{2/3}$), and the

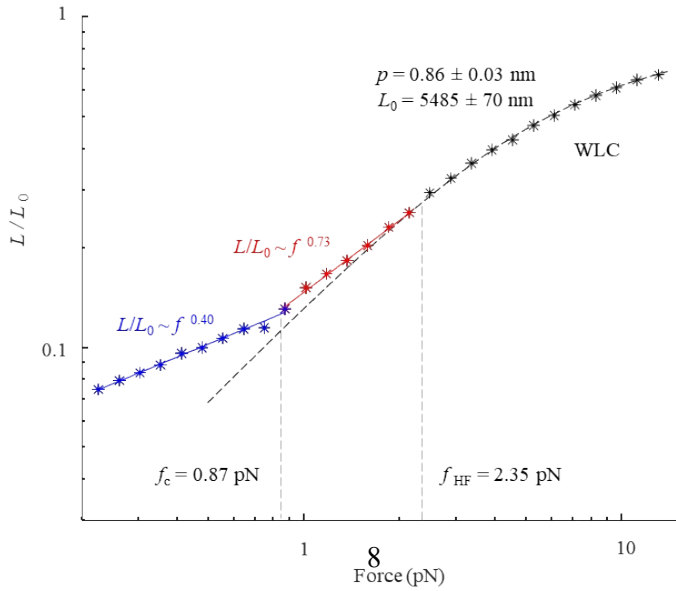

Fig. S8. Representative analysis of single-chain force-extension data (polynorbornene in 9:1 toluene-ethanol solution) to extract single chain scaling and elasticity behavior.

data below 0.87 pN display super swollen behavior with scaling exponent of 0.40 (which is much smaller than the 2/3).

S8. Supplementary data

The supplementary data includes additional single-chain data that complements the results in the main text of the manuscript and further highlight the unique single-chain scaling behavior of individual polymers even under solvent identical conditions.

S8.1. Force-extension data for the additional polynorbornenes under toluene, 9:1 toluene-ethanol, and 8:2 toluene-ethanol show consistent sensitivity of the single-chain elasticity to solvent

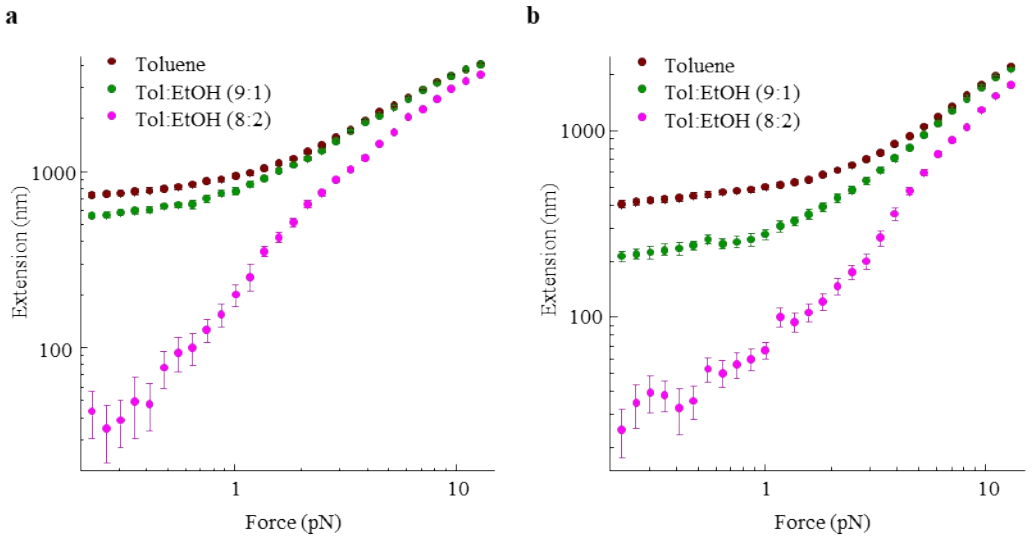

Fig. S9. Single-chain extension-versus-force trajectories of two different polynorbornenes under different solvent environments.

environment as in **Fig. 2(a)**.

S8.2. The heterogeneity in scaling behavior for polynorbornene in a good solvent (toluene) displays a distinct correlation with polymer contour length, suggesting this behavior is not a consequence of their chain length/molecular weight dispersion.

Fig. S10. Scatter plot of scaling exponent with the polymer contour length (L_0) for individual polynorbornene polymers in toluene.

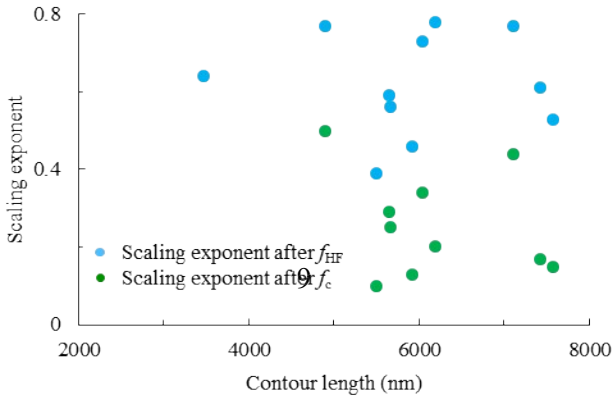

S8.3. The heterogeneity in the scaling behavior of polynorbornene in a good solvent (toluene) is not a consequence of our scheme for growing surface-grafted polynorbornenes under confinement (Fig. S1). While the catalyst environment in our scheme is slightly perturbed compared to solution polymerization using Grubbs catalyst, it may affect the real-time polymerization dynamics. However, this particular polymerization scheme is not expected to result in differences in single-chain elasticity of the individual polymers after the growth, as the equilibrium polymer conformations are expected to depend on its intrinsic properties (such as chemical structure, branching, and end groups) and the environmental properties (such as solvent, temperature, and pH) and not on its synthetic route. To further support this, we performed a control measurement of growing surface-grafted polynorbornenes from G2 immobilized on the glass coverslip, followed by the subsequent attachment of the magnetic particle to the pre-grown polymer. The representative single-chain elasticity data in this measurement still exhibit heterogeneity among individual polynorbornenes in toluene, further supporting the observed behavior and not a consequence of the growth scheme.

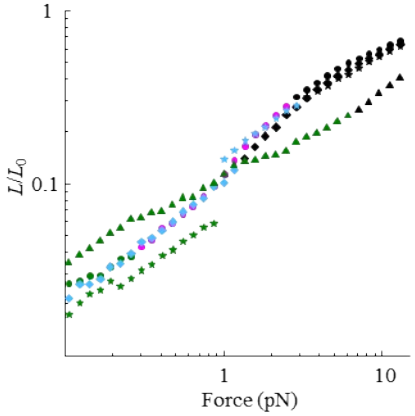

Fig. S11. Single-chain elasticity profiles in toluene of polynorbornene polymers pre-grown via G2 catalyst immobilized on glass before magnetic bead immobilization.

S8.4. The relaxation and stretching profiles for individual polynorbornenes in toluene overlap within the experimental error of extension measurement, reflecting no distinct hysteresis in single-chain elasticity and scaling behavior.

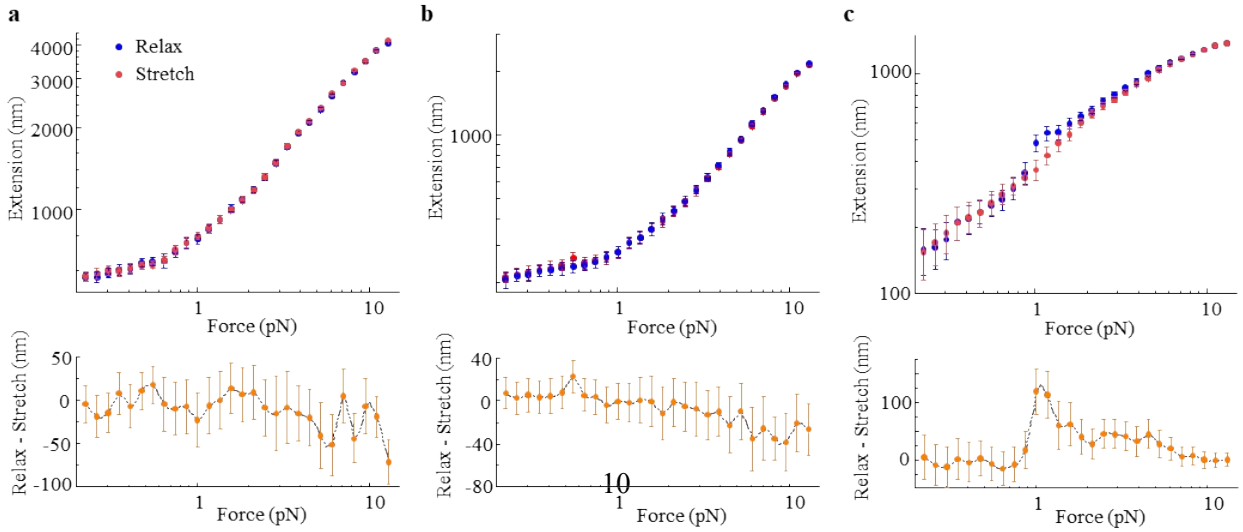

Fig. S12. Single-chain force-extension behavior of three individual polynorbornene chains under relaxation and stretching measurements in toluene.

S8.5. The relaxation and stretching profiles for individual polynorbornenes in 9:1 toluene-ethanol overlap within the experimental error of extension measurement, reflecting no distinct hysteresis in single-chain elasticity and scaling behavior

S8.6. The relaxation and stretching profiles for individual polynorbornenes in 8:2 toluene-ethanol show distinct hysteresis in single-chain elasticity and scaling behavior for 11/15 additional polymers studied.

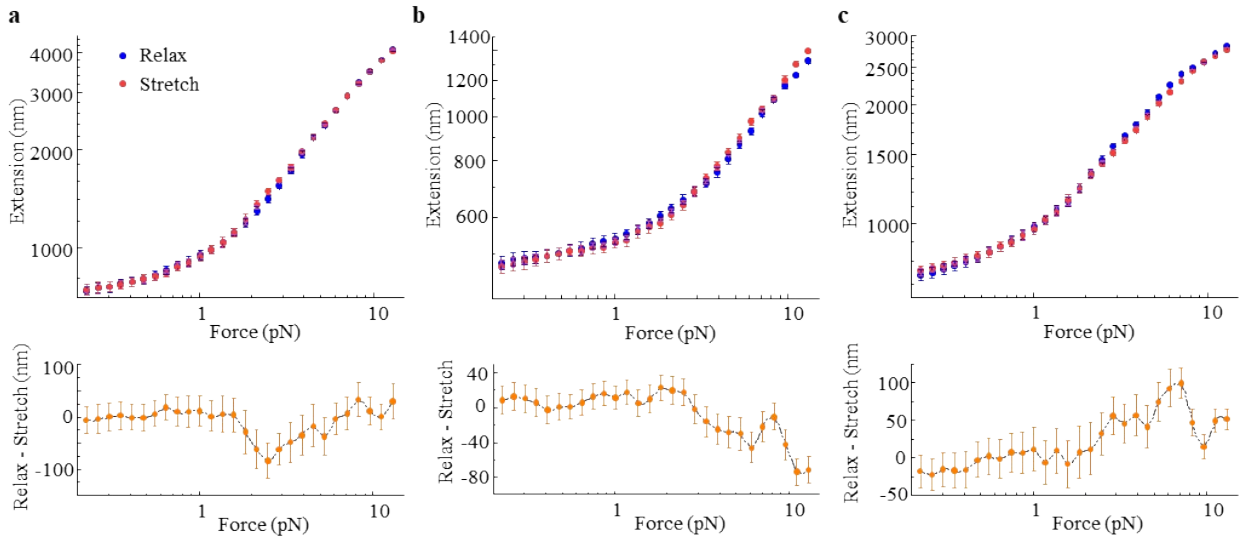

Fig. S13. Single-chain force-extension behavior of three individual polynorbornene chains under relaxation and stretching measurements in 9:1 toluene-ethanol mixture.

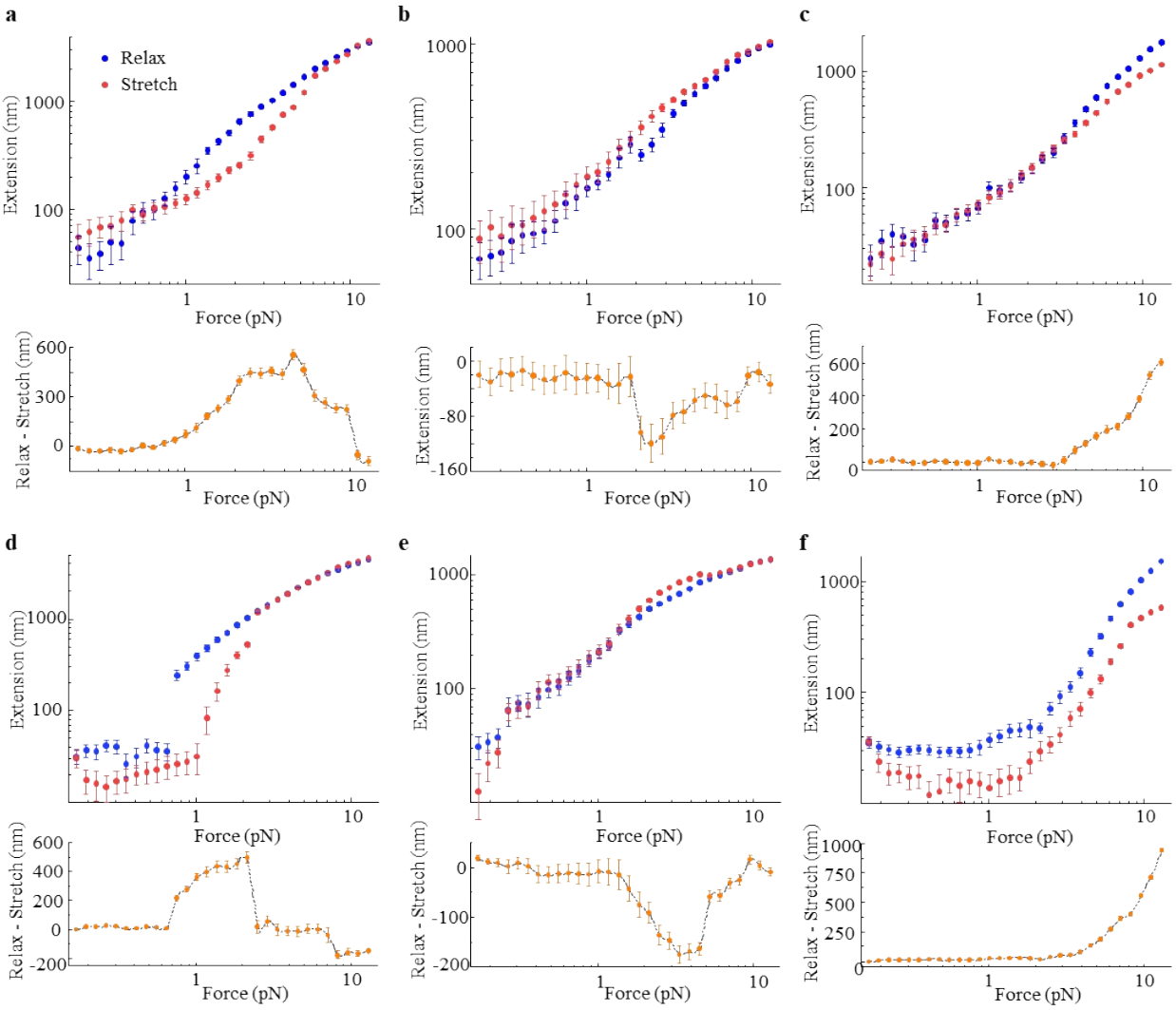
a
b
c
d
e
f
Relax
Stretch
Extension (nm)
Relax - Stretch (nm)
Force (pN)
1000
100
600
300
0
-80
-160
400
200
-200
750
500
250

246

247

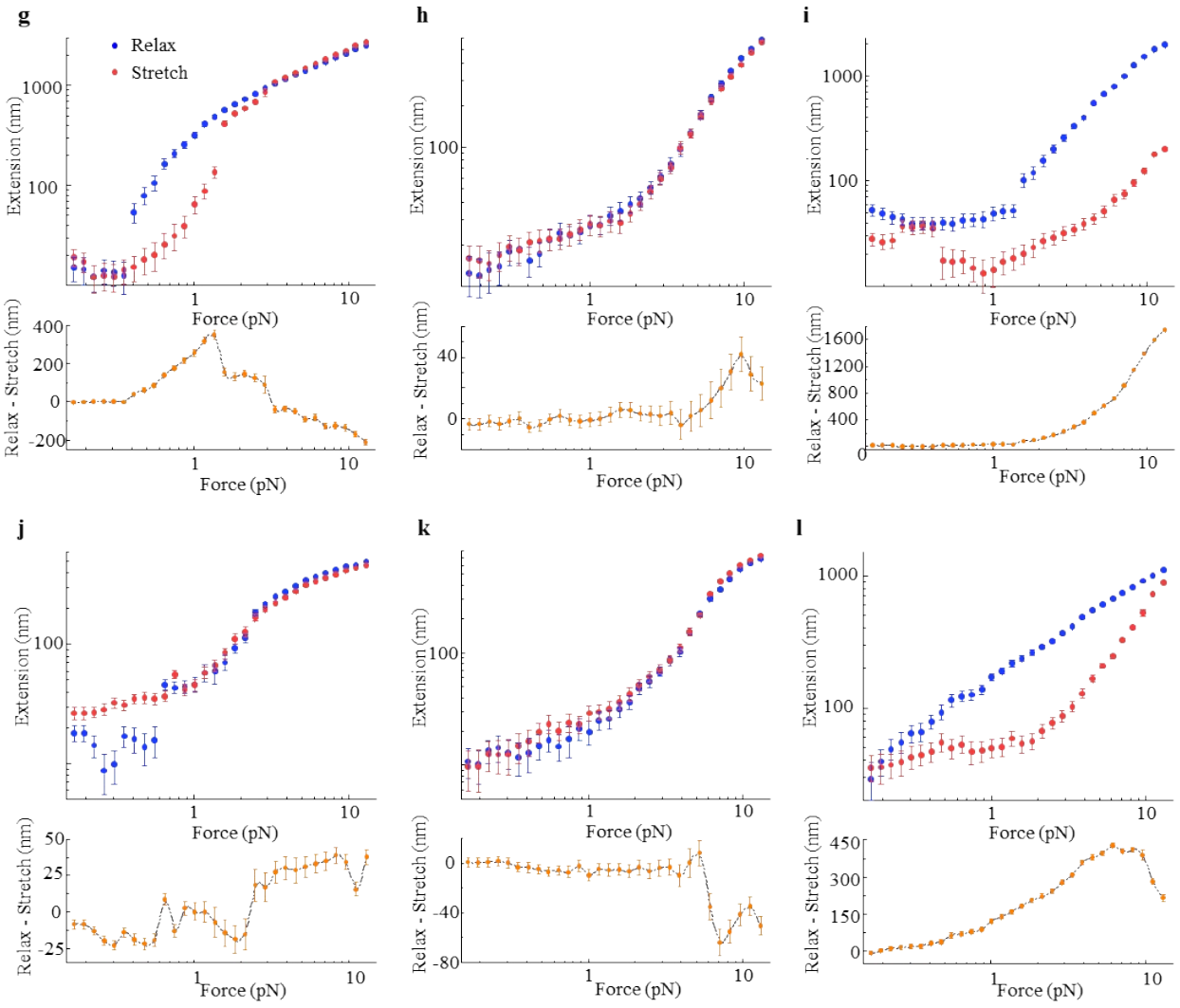
g
h
i
j
k
l
Relax
Stretch
Extension (nm)
Relax - Stretch (nm)
Force (pN)

248

Fig. S14. (**a – o**) Single-chain force-extension behavior of individual polynorbornene chains under relaxation and stretching measurements in 8:2 toluene-ethanol mixture.

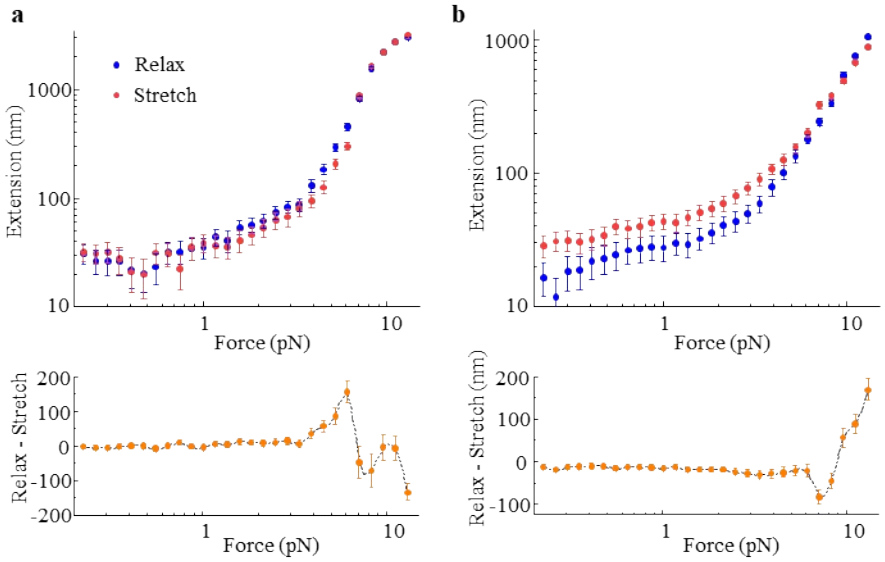

Fig. S15. Single-chain force-extension behavior of two individual polynorbornene chains under relaxation and stretching measurements in 7:3 toluene-ethanol mixture.

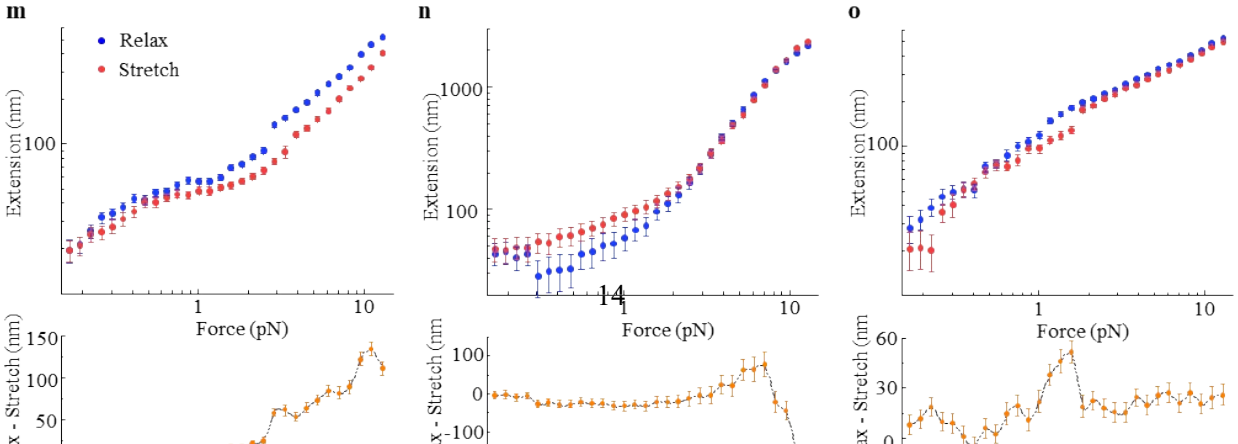

S8.7. The relaxation and stretching profiles for individual polynorbornenes in 7:3 toluene-ethanol show distinct hysteresis in single-chain elasticity and scaling behavior.

S8.8. The relaxation and stretching profiles for individual polynorbornenes in 6:4 toluene-ethanol show distinct hysteresis in single-chain elasticity and scaling behavior for 11/14 individual polymers studied.

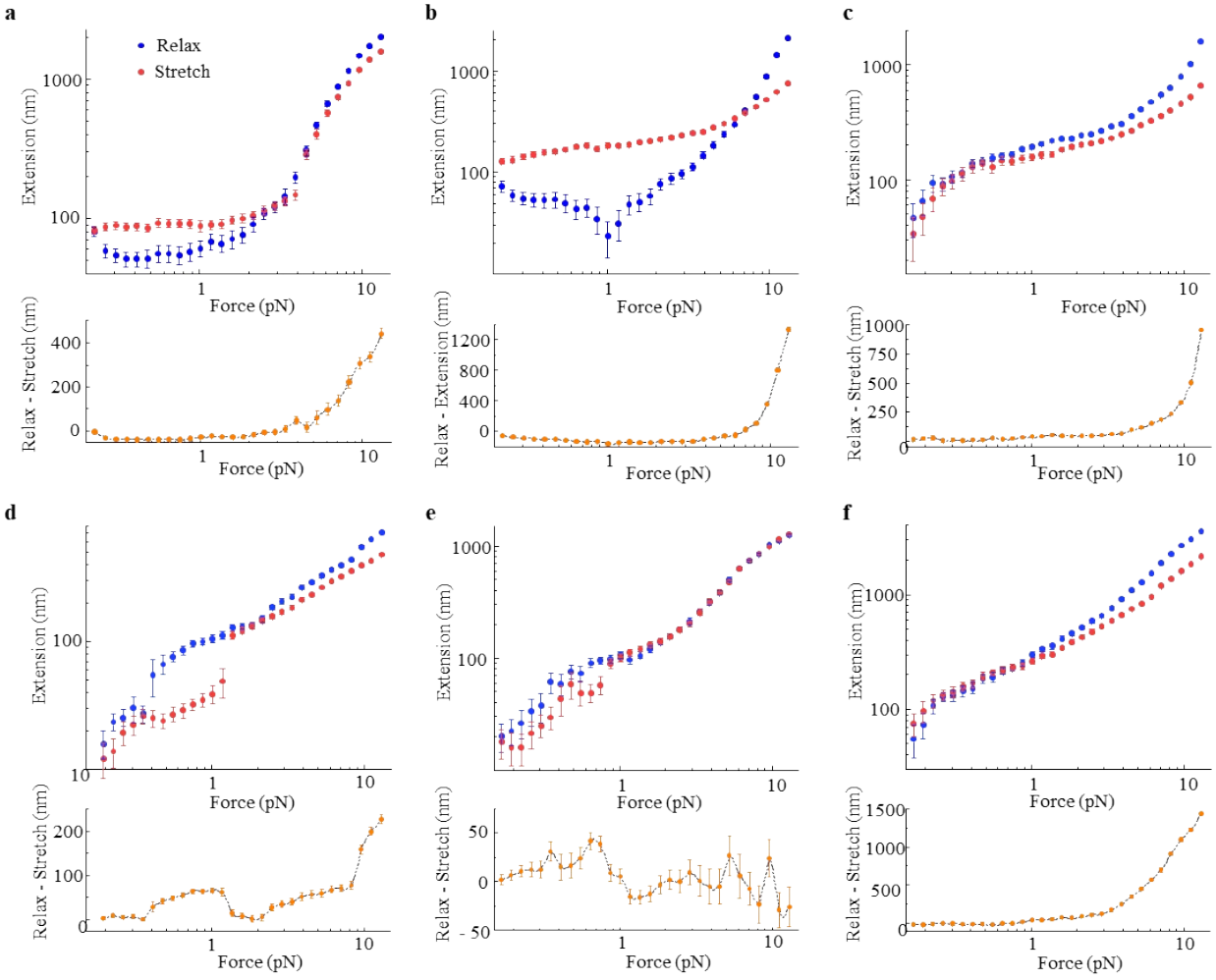

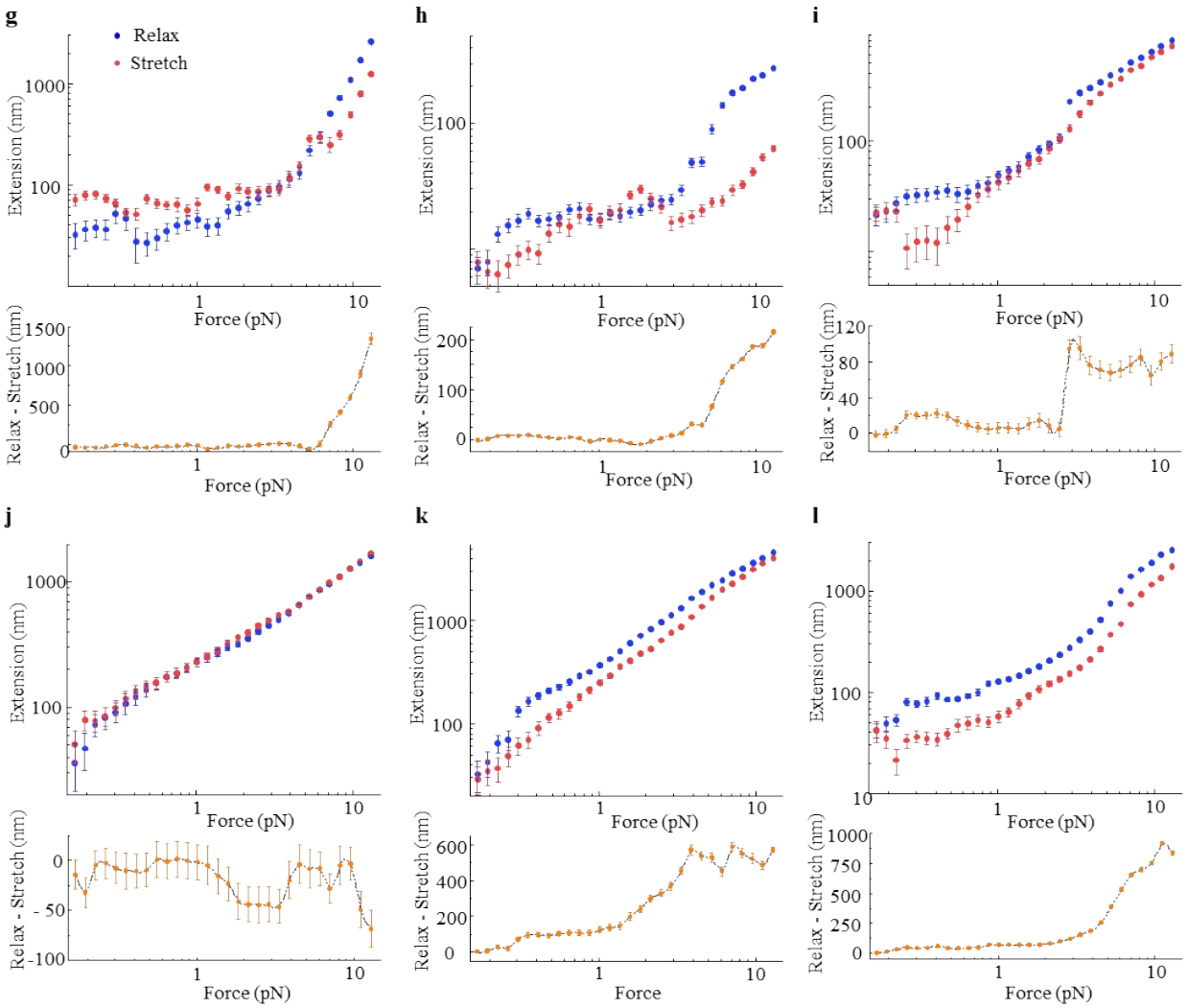
g
h
i
j
k
l
Relax
Stretch
Extension (nm)
Relax - Stretch (nm)
Force (pN)
Force

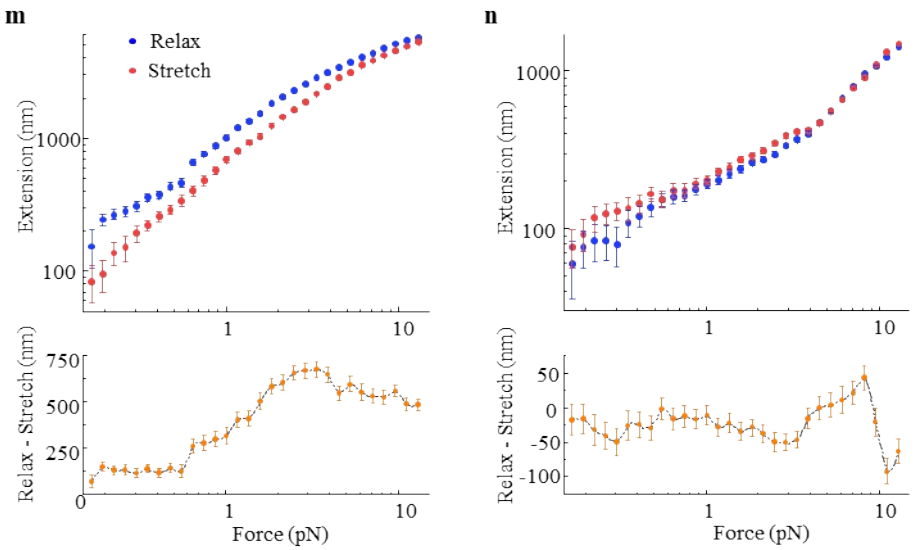

Fig. S16. (**a – n**) Single-chain force-extension behavior of individual polynorbornene chains under relaxation and stretching measurements in 6:4 toluene-ethanol mixture.

S8.9. Th exemplary measurements with multiple relaxation and stretching cycles in Toluene (i.e., good solvent) display reproducible single-chain elasticity profiles with no hysteresis.

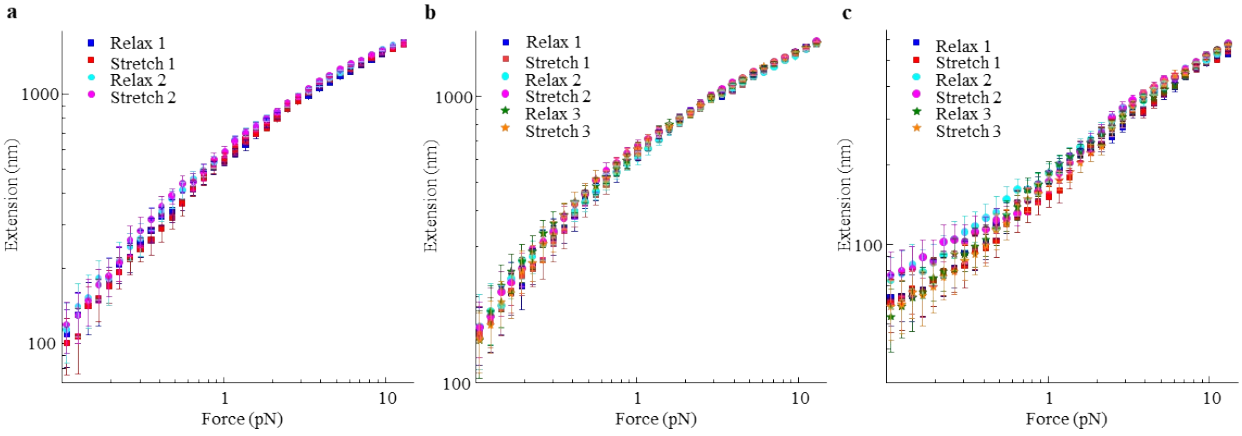

Fig. S17. Single-chain elasticity profiles of independent polynorbornene polymers in toluene under multiple relaxation and stretching cycles.

S8.10. Th exemplary measurements with multiple relaxation and stretching cycles in 8:2 toluene-ethanol solvent display hysteresis in single-chain elasticity profiles.

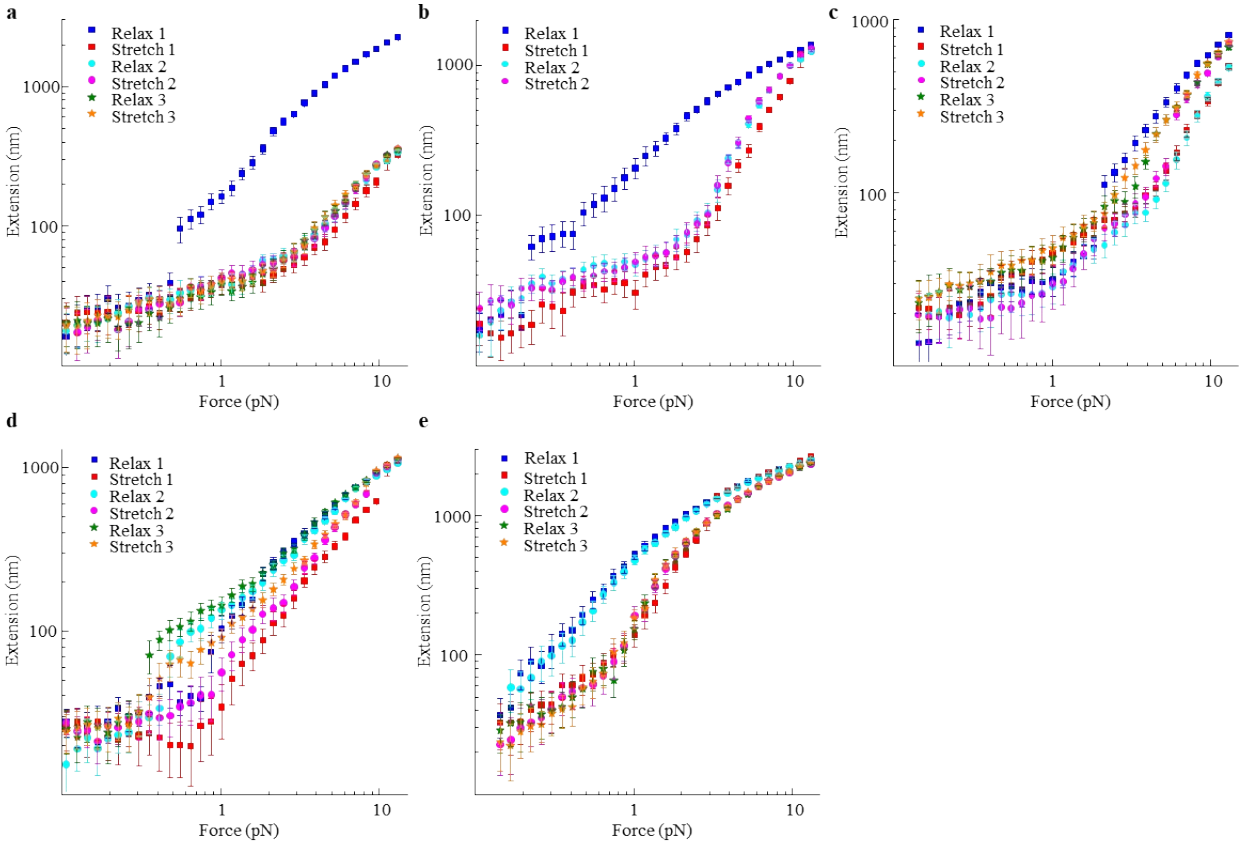

Fig. S18. Single-chain elasticity profiles of independent polynorbornene polymers in 8:2 toluene-ethanol under multiple relaxation and stretching cycles.

S8.11. Th exemplary measurements with multiple relaxation and stretching cycles in 6:4 toluene-

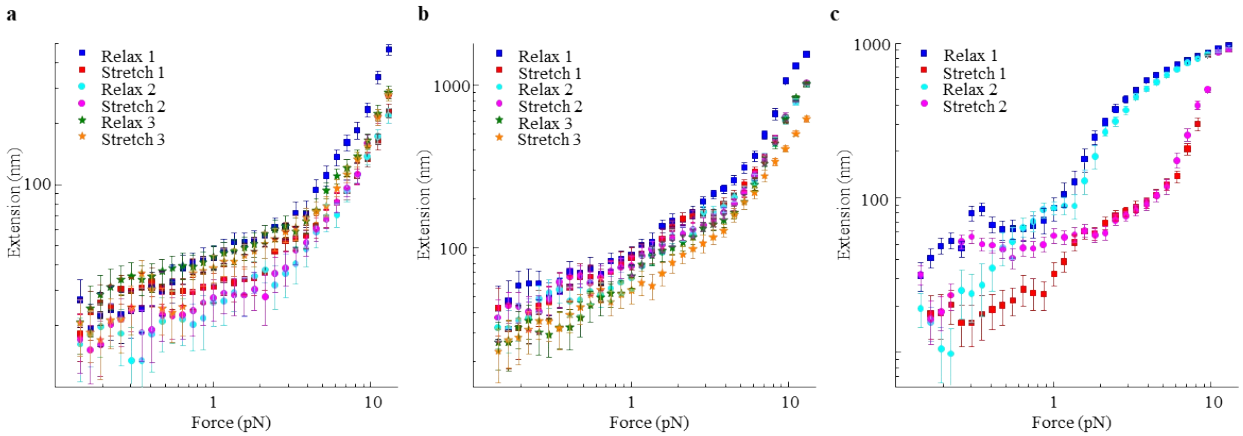

Fig. S19. Single-chain elasticity profiles of independent polynorbornene polymers in 6:4 toluene-ethanol under multiple relaxation and stretching cycles.

ethanol solvent display hysteresis in single-chain elasticity profiles.

S9. References

1. C. Liu, K. Kubo, E. Wang, K.-S. Han, F. Yang, G. Chen, F. A. Escobedo, G. W. Coates and P. Chen, *Science*, 2017, **358**, 352-355.
2. S. Baral, C. Liu, U. K. Chakraborty, K. Kubo, X. Mao, G. W. Coates and P. Chen, *Chem*, 2021, **7**, 2175-2189.
3. S. Baral, C. Liu, X. Mao, G. W. Coates and P. Chen, *ACS Cent. Sci.*, 2022, **8**, 1116-1124.
4. J. Lipfert, X. Hao and N. H. Dekker, *Biophys. J.*, 2009, **96**, 5040-5049.
5. A. J. W. te Velthuis, J. W. J. Kerssemakers, J. Lipfert and N. H. Dekker, *Biophys. J.*, 2010, **99**, 1292-1302.
6. Y. Seol and K. C. Neuman, in *Single Molecule Analysis: Methods and Protocols*, eds. E. J. G. Peterman and G. J. L. Wuite, Humana Press, Totowa, NJ, 2011, DOI: 10.1007/978-1-61779-282-3_15, pp. 265-293.
7. A. Dittmore, D. B. McIntosh, S. Halliday and O. A. Saleh, *Phys. Rev. Lett.*, 2011, **107**, 148301.
8. M. Grandbois, M. Beyer, M. Rief, H. Clausen-Schaumann and H. E. Gaub, *Science*, 1999, **283**, 1727-1730.
9. Dustin B. McIntosh, G. Duggan, Q. Gouil and Omar A. Saleh, *Biophys. J.*, 2014, **106**, 659-666.